Crystal structure of the wide-spectrum binuclear zinc β-lactamase from *Bacteroides fragilis*

Nestor O Concha[1], Beth A Rasmussen[2], Karen Bush[2] and Osnat Herzberg[1]*

Background: The metallo-β-lactamase from *Bacteroides fragilis* hydrolyzes a wide range of β-lactam antibiotics, and is not clinically susceptible to any known β-lactamase inhibitors. *B. fragilis* is associated with post-surgery hospital infections, and there has been a recent report of plasmid-mediated dissemination of the enzyme. Effective inhibitors are therefore urgently needed. Knowledge of the three-dimensional structure will aid in the drug design effort.

Results: The crystal structure of the enzyme has been determined by using multiwavelength anomalous diffraction at the zinc absorption edge and refined to 1.85 Å resolution. The structure is a four-layer α/β/β/α molecule. The active site, found at the edge of the β sandwich, contains a binuclear zinc center with several novel features. One zinc is tetrahedrally coordinated, the other has a trigonal bipyramidal coordination; a water/hydroxide molecule serves as a ligand for both metals. The residues that coordinate the two zincs are invariant in all metallo-β-lactamases that have been sequenced, except for two conservative replacements. Despite the existence of the pattern for binuclear zinc binding, the reported structure of the *Bacillus cereus* enzyme contains only a single zinc.

Conclusions: Structural analysis indicates that affinity for the penta-coordinated zinc can be modulated by neighboring residues, perhaps explaining the absence of the second zinc in the *B. cereus* structure. Models of bound substrates suggest that the active-site channel can accommodate a wide variety of β-lactams. We propose that the zinc cluster prepares an hydroxide, probably the hydroxide that ligates both zincs, for nucleophilic attack on the carbonyl carbon atom of the β-lactam. The resulting negatively charged tetrahedral intermediate implicated in catalysis is stabilized by an oxyanion hole formed by the side chain of the invariant Asn193 and the tetrahedral zinc.

Addresses: [1]Center for Advanced Research in Biotechnology, University of Maryland Biotechnology Institute, 9600 Gudelsky Drive, Rockville, MD 20850, USA and [2]Wyeth-Ayerst Research, Lederle Laboratories, Pearl River, NY 10965, USA.

*Corresponding author.
E-mail: osnat@elan1.carb.nist.gov

Key words: binuclear zinc, metallo-β-lactamase, X-ray crystallography, zinc β-lactamase

Received: 18 April 1996
Revisions requested: 16 May 1996
Revisions received: 28 May 1996
Accepted: 28 May 1996

Structure 15 July 1996, 4:823–836

Introduction

β-Lactam antibiotics are effective and widely used compounds against pathogenic bacterial infections. They inactivate key enzymes of the bacterial cell wall synthesis and repair pathways, leading to defective cell walls and, eventually, cell death [1]. It is the production of β-lactamases [2], enzymes that catalyze the hydrolysis of the amide bond of the β-lactam ring, that provides the major bacterial defense mechanism against this type of antibiotic. On the basis of amino acid sequence homology, β-lactamases have been divided into four classes, A–D [3–5]. Classes A, C and D share an active-site serine residue and are collectively termed the serine β-lactamases. The hydroxyl group of the serine residue mounts the nucleophilic attack on the carbonyl carbon atom of the β-lactam ring. In contrast, the class B enzymes require metal ions for catalytic activity [6,7], and their amino acid sequences lack the Ser-X-X-Lys fingerprint typical of the active sites of the serine β-lactamases [8–14]. *In vivo*, class B β-lactamases probably function in the Zn^{2+}-bound form, but activity is also observed in the Cd^{2+}- or Co^{2+}-bound forms of the enzyme [7,15,16]. By analogy with other metallo-hydrolases [17,18], the catalytic mechanism may involve a hydrolytic water molecule with enhanced nucleophilicity due to its proximity to the metal ion.

The first metallo-β-lactamase to be identified was from *Bacillus cereus*. For as long as this enzyme was the only metallo-β-lactamase known, the class B enzymes were considered somewhat obscure and posed little clinical threat. With the rapid identification of new metallo-β-lactamases and the realization that they can hydrolyze a wide range of substrates, including cephamycins and imipenem that are resistant to the serine β-lactamases [16,19–21], the clinical risks became apparent. Moreover, the metallo-enzymes show little or no susceptibility to traditional β-lactamase inhibitors, such as clavulanic acid or sulbactam [16,19]. The metallo-enzymes are inhibited by the metal chelators EDTA and 1,10-o-phenantroline [6,7,14–16,22, 23], but it is yet to be shown that these can be used as lead compounds for the development of specific inhibitors. The antibiotic tazobactam inactivates metallo-β-lactamases, but not at a level that is clinically useful [24].

To date, the amino acid sequences of metallo-β-lactamases from *B. cereus* [8], *Bacteroides fragilis* [9,10], *Aeromonas hydrophila* [11,12], *Xanthomonas maltophilia* [13], and *Serratia marcescens* [14] have been determined. Only the first four proteins share a level of sequence identity indicative of an evolutionary relationship (25–37% identity). Thus, as more sequences of metallo-β-lactamases become available reclassification may be required.

Early work on the metallo-β-lactamase from *B. cereus* indicated that the enzyme binds one zinc ion with high affinity, and a second with much lower affinity (with a K_d in millimolar range) [7]. Substrate hydrolysis correlated mostly with the metal binding at the site of higher affinity; spectroscopic measurements implicated a cysteine residue in metal binding [7]. ^{1}H NMR spectroscopy further implicated three histidine residues as ligands of the high affinity metal ion, and a fourth histidine as a ligand of the low affinity metal ion [25]. More recently, the determination of the crystal structure of the enzyme from *B. cereus* revealed a single Zn^{2+} coordination to three invariant histidine residues [26]. The crystal structure also showed that the Zn^{2+} binds at the interface between two β sheets, and suggested that an invariant aspartate residue, Asp90, located close to the Zn^{2+} acts as the general base that accepts the proton from the hydrolytic water molecule.

The metallo-β-lactamases that have been studied span a wide range of catalytic efficiencies [27]. The enzymes with the narrowest specificity profile are from the group of *Aeromonas* species. The enzyme from *A. hydrophila* has only two good substrates, imipenem and ampicillin, and it is inhibited by cefoxitin [19,20]. Its ability to hydrolyze imipenem, a penicillin with an α-substituent on the β-lactam ring, is the main cause of concern. The *B. fragilis* enzyme, the subject of this study, exhibits the broadest spectrum for different substrates and the most efficient activity [16,19–21]. k_{cat}/K_m values for a sample of 25 penicillins and cephalosporins vary from ~10^5 to ~10^7 $M^{-1}s^{-1}$ [16].

B. fragilis, a gram-negative anaerobe, is considered one of the most important pathogens in polymicrobial infections in humans [28–30]. The proliferation of the bacteria in nosocomial infections, combined with the broad-spectrum substrate profile of its metallo-β-lactamase, the lack of potent inhibitors, and the report of plasmid-mediated dissemination of the enzyme [31] (K Bandoh, W Watanabe, Y Muto, Y Tanaka, N Kato, K Ueno, [abstract 945], 31st Interscience Conference on Antimicrobial Agents and Chemotherapy, Tokyo, 1991) underscore the need for better understanding of the catalytic mechanism and the basis for substrate specificity. We present here, the refined, high resolution crystal structure of the *B. fragilis* metallo-β-lactamase, showing that the active site contains a binuclear (Zn^{2+}-Zn^{2+}) center. The three-dimensional view of the active site together with modeling of bound substrates provide the structural basis for future drug design efforts.

Results and discussion

Quality of the model

The soluble polypeptide chain of the metallo-β-lactamase from *B. fragilis* consists of residues 18–249 (the first 17 amino acids constitute the signal peptide). The crystal structure provides two crystallographically independent views of the molecule, termed A and B. These are related to each other by a non-crystallographic rotation axis of 179.6°. The model for molecule B includes all the amino acid residues except for 48 and 49, which are associated with a region of low electron density. In molecule A, these two residues and the first two N-terminal residues are disordered. The model includes a total of 527 water molecules, two zinc ions and one sodium ion per molecule. The crystallographic R factor ($R=\Sigma_h||F_o|-|F_c||/\Sigma_h|F_o|$, where $|F_o|$ and $|F_c|$ are the observed and calculated structure factor amplitudes, respectively) is 0.167 for 34 597 reflections in the resolution range 8.0–1.85 Å for which $F>2\sigma(F)$. The estimated mean coordinate error is 0.2 Å, as calculated with SIGMAA [32]. The root mean square (rms) deviation from ideal bond length and bond angle values of the standard geometry, compiled by Engh and Huber [33], are 0.02 Å, and 1.9°, respectively. The rms difference between the α carbon atom positions of the two molecules in the asymmetric unit is 0.5 Å [34]; the largest differences are at residues Ile24–Asp26 (4.7 Å difference at Asp26). Two other large differences between the two molecules occur at Glu47, adjacent to the disordered dipeptide 48–49 (1.2 Å difference), and at the C-terminal Pro249 (2.8 Å difference). These differences are associated with regions of high crystallographic temperature factors. Residues Ile24–Asp26, located remotely from the active site, are involved in crystal contacts in molecule A but not in molecule B. It is the difference in the local environment that determines which conformation has been adopted. The environment in molecule A is determined by two key interactions: a water molecule bridging the two carboxylate groups of a symmetry related Asp26 pair; and an intermolecular contact between Ser25 Oγ and Met51 Sδ (3.0 Å). In contrast, both Asp26 and Ser25 of molecule B form intramolecular interactions. The carboxylate group of Asp26 interacts with the amino group of Lys23, and Ser25 Oγ interacts with Ile28 N. When the deviating residues listed above are omitted from the comparison, the rms difference between the two molecules is 0.3 Å.

Overall structure

The metallo-β-lactamase from *B. fragilis* is an α+β protein (Fig. 1), of the four-layered α/β/β/α class. However, the topology of this enzyme is quite distinct from some other members of this class, including DNase I [35], exonuclease III [36], and the N-terminal nucleophile family [37].

Figure 1

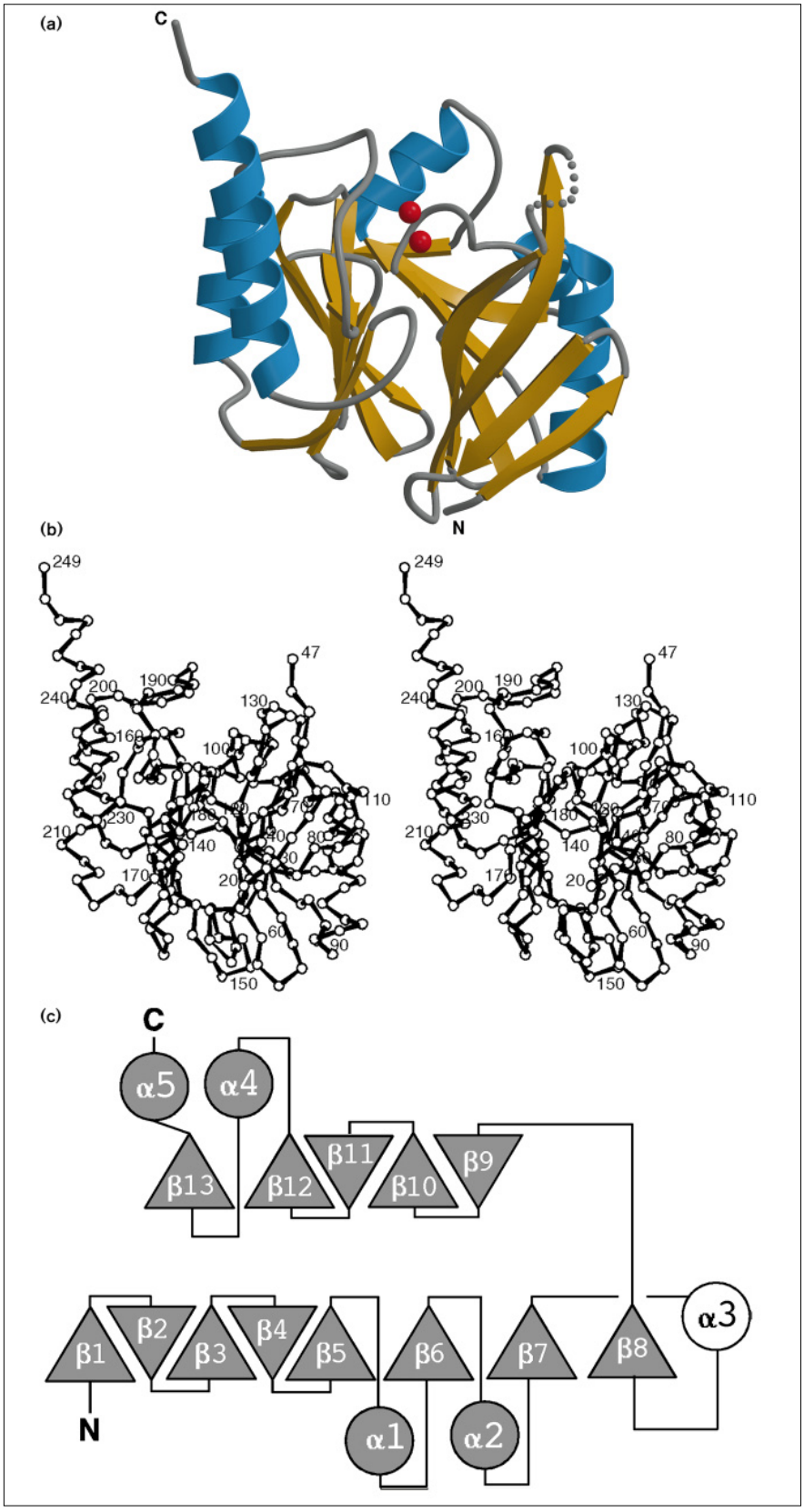

The fold of *B. fragilis* metallo-β-lactamase. (a) Ribbon diagram highlighting secondary structure motifs. Helices and β strands are colored blue and gold, respectively. The zinc metal ions in the active site are shown as red spheres and are located at the top edge of the β sandwich. The dotted line corresponds to the positions of the two conformationally disordered residues (48 and 49) in the vicinity of the active site. (The figure was generated with Molscript [69] and rendered with Raster3D [70] using the 2.0 version [71] and a TCL-TK front-end developed by H Gilson [unpublished program].) (b) Stereoscopic representation of the trace of the Cα atom positions, shown in the same orientation as (a). The position of every tenth residue is numbered. (c) Topographical diagram of the arrangement of the secondary structure elements of β-lactamase. Triangles represent β strands and circles represent α helices, the N and C termini are marked. To indicate that it is not part of the α/β layer α3 is shown in white.

Consistent with the amino acid sequence homology, the overall fold of the metallo-β-lactamase is the same as that of the enzyme from *B. cereus* [26]. However, an additional β strand (β8 in Fig. 1c) has been assigned in the N-terminal sheet of the *B. fragilis* metallo-β-lactamase and the topology scheme is not the same. This probably reflects differences in topology analysis rather than genuine differences in the tracing of the polypeptide chain. For example, α3 in the current study is not part of the β sandwich, and α4 and α5 are depicted as being antiparallel. Carfi *et al.* [26] discussed the symmetry between the two α/β layers. However, the symmetry is not exact; the pair of helices that pack against the sheet of the N-terminal α/β layer (α1 and α2 in Fig. 1c) run parallel to each other, whereas the equivalent helices (α4 and α5) that pack against the C-terminal β sheet run antiparallel to each other. The last two strands of the first β-sheet, β7 and β8 are connected by a large helix-containing loop, with the helix (α3) running perpendicular to the β-sheet and not contacting the first two helices.

The interfaces between sheet and helices, and between the two sheets are dominated by hydrophobic interactions. However, the packing is not perfect and a total of six water molecules and a sodium cation, that are inaccessible to bulk solvent, were observed underneath the lining of the active-site depression. These molecules occupy three distinct cavities. The largest cavity contains three water molecules and the sodium cation, the second to the largest contains two water molecules, and the smallest cavity is occupied by a single water molecule. Asp69, which as discussed later exhibits an unusual conformation, is wedged between the two former cavities. The buried solvent molecules and Asp69 may have functional role, this is yet to be investigated.

The active site

The loops which connect secondary structure units on one side of the molecule (located at the bottom in the view presented in Fig. 1a,b) are systematically shorter, compared with the more extensive loops on the opposite side (top of Fig. 1a,b). The active site is associated with the region containing the large loops, at the edge of the β sandwich. The location of the active site in the crystal structure of the metallo-β-lactamase from *B. cereus* is the same, except that it only contains one zinc [26], in contrast to the *B. fragilis* enzyme which contains two zinc ions. All amino acid residues that coordinate to the two zinc ions reside on loops and turns. Interestingly, the location of the metal ion in exonuclease III [36] is similar, despite differences in the topology. Similarly, the active site of the N-terminal nucleophile family is also observed within the interface between the two β sheets [37].

The two zinc ions are located 3.5 Å apart, at the bottom of a groove (Fig. 2). The first zinc ion, Zn1, is coordinated to four ligands in a tetrahedral geometry (Table 1, Fig. 3); three histidine residues (His99 Nε, His101 Nδ, and His162 Nε) and a solvent molecule that has been refined as a water (Wat1). The second zinc, Zn2, is coordinated to five ligands in a distorted trigonal bipyramidal geometry: three protein residues (Asp103 Oδ2, Cys181 Sγ and His223 Nε); and two water molecules (Wat1 and Wat2). The apical positions of the trigonal bipyramid are occupied by Asp103 Oδ2 and Wat2 (termed the apical water throughout), and the equatorial positions are occupied by Cys181 Sγ, His223 Nε, and Wat1. The proximity of Wat1 to both zinc ions indicates that most likely this is a hydroxide (termed the shared hydroxide). In addition to coordination to the two zinc ions, the shared hydroxide forms an electrostatic interaction with Asp103 Oδ1 indicating that they share a proton. Finally, Cys181 is presumably also negatively charged. This is the first example of a cysteine residue that coordinates to a zinc ion in a binuclear zinc center.

There are intricate electrostatic interactions between the zinc ligands and nearby protein groups and solvent molecules that assure the precise positions and orientations of the ligands. The type of electrostatic interactions between the imidazole groups (His99, His101, His162 and His223) and other protein residues is consistent with there being a

Figure 2

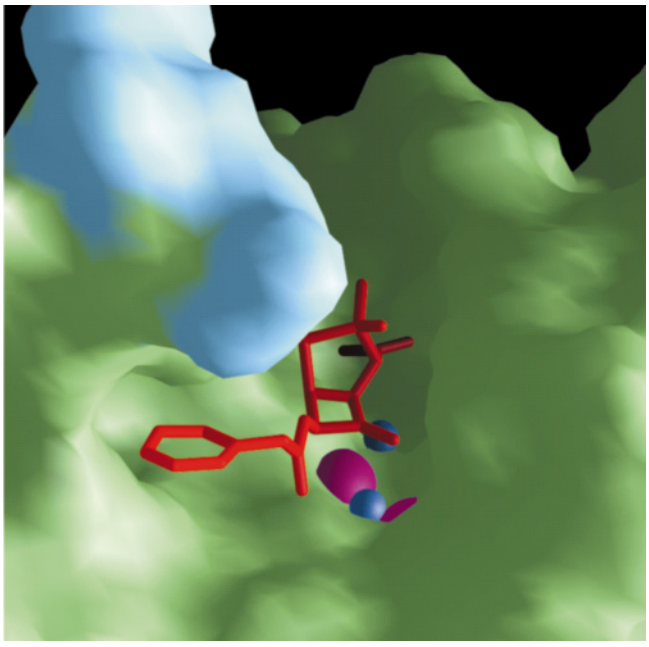

The active site of the *B. fragilis* metallo-β-lactamase. The molecular surface of the enzyme is depicted together with a model of a bound molecule of benzylpenicillin (colored red). The benzyl side chain fits into a hydrophobic pocket. The zinc ions are represented as magenta spheres and two key water molecules as blue spheres. The disordered residues, 48 and 49, and the side chain of Glu50 are colored light blue. (The figure was generated with GRASP [72].)

Table 1

Zinc ligands.*

Zn1 (tetrahedral)‡		Zn2 (trigonal bipyramidal)§	
His99 Nϵ	2.1/2.2	Asp103 Oδ†	2.3/2.1
His101 Nδ	2.0/2.1	Cys181 Sγ	2.3/2.4
His162 Nϵ	2.0/2.0	His223 Nϵ	2.1/2.2
Wat1/Wat3†	1.9/1.9	Wat1/Wat3†	2.1/2.2
		Wat2/Wat4	2.3/2.2

*Distances to the metal (in Å) are quoted for the two molecules in the asymmetric unit. Wat1 and Wat2 bind to molecule A and Wat3 and Wat4 bind to molecule B. †Distances between Asp103 Oδ1 and Wat1/Wat3 are 2.7/2.5 Å. ‡Average ligand–Zn–ligand angle, 109°. §Average ligand–Zn–ligand angle for equatorial atoms (Cys181 Sγ, His223 Nϵ and Wat1), 120°; angle between ligands at the apices (Asp103 Oδ and Wat2), 164°; average angle between ligands at the apices and equatorial ligands, 90°.

protonated form of each of the non-coordinating nitrogen atoms: His99 Nδ interacts with Asn98 Oδ (2.7 Å) (while Asn98 Nδ interacts with Ile167 O, 2.7 Å); His101 Nε interacts with Asp196 Oδ (2.7 Å); His162 Nδ interacts with a water molecule Wat7 (3.0 Å) which in turn interacts with the two main-chain carbonyl oxygen atoms of Ile191 (2.8 Å) and Asn193 (2.8 Å); His223 Nδ interacts with Ser53 O (2.8 Å). The non-histidine protein ligands, Cys181 and Asp103, interact with tightly bound internal water molecules, and this may help modulate their charge state. Cys181 is bridged by Wat9 to the carboxylate group of Asp69 (3.2 Å), and Asp103 interacts with Wat11 (2.7 Å). Watt 11 in turn interacts with the sodium cation that forms a buried ion pair with the Asp69 carboxylate group. The second molecule in the asymmetric unit exhibits the same arrangement of coordination and second shell interactions.

Zinc clusters have been observed in the active sites of other enzymes [38]. Seven structures that contain at least two zinc ions have been examined: alkaline phosphatase [39]; phosphotriesterase [40]; Klenow fragment of DNA polymerase I [41]; P1 nuclease [42]; phospholipase C [43]; aminopeptidase [44]; and leucine aminopeptidase [45]. The distance between a pair of zinc ions in these structures varies between 2.9–3.9 Å, thus the distance observed in the β-lactamase structure is well within this range (3.5 Å). Although the arrangement of ligands in the *B. fragilis* enzyme is unique among binuclear zinc enzymes, there is one notable common feature; there is always a negatively charged group, either a carboxylate, a hydroxide or a phosphate anion shared by the two zinc ions.

The structurally-based amino acid sequence alignment of the various metallo-β-lactamases reveals that most, if not all, enzymes contain the hallmark for a binuclear-zinc center (Fig. 4). Conforming to the numbering scheme of the β-lactamase from *B. fragilis*, three ligands are located

Figure 3

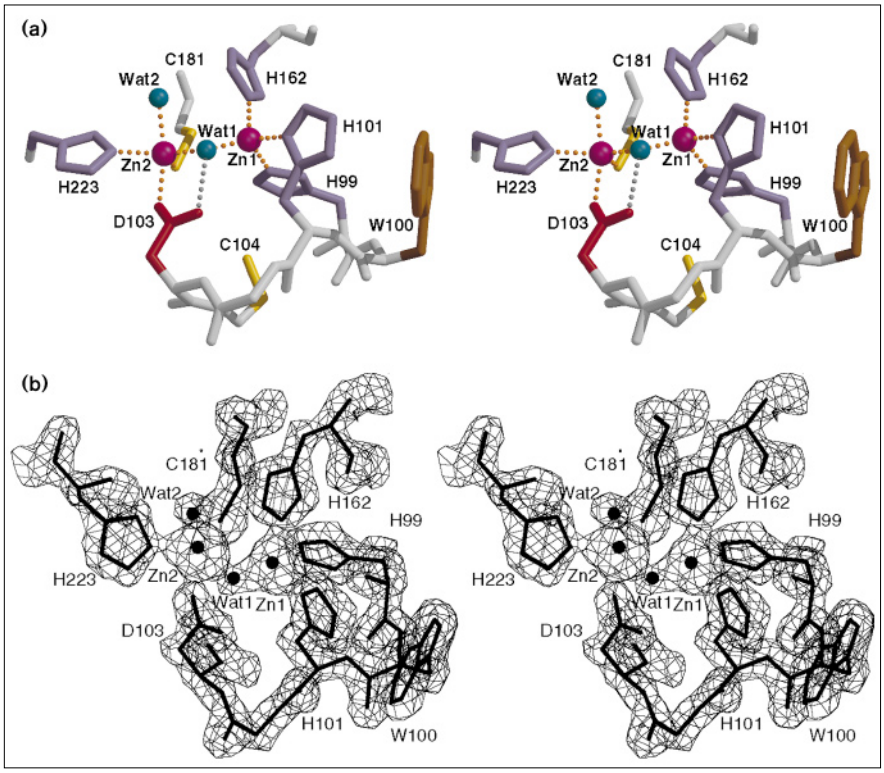

The environment of the binuclear zinc centre in the metallo-β-lactamase from *B. fragilis*. **(a)** Stereoscopic representation of the atomic model of the active site. The zinc and metal-bound solvent molecules are represented as magenta and turquoise spheres, respectively. The color-coding used in this figure is used throughout. Main-chain bonds are colored gray, negatively charged residues are colored in varying intensities of red, positively charged residues are in purples, hydrophobic residues in greens, browns and yellows, and hydrophilic residues are shown in pinks and oranges. Zinc–ligand interactions are shown as orange dotted lines. Other key electrostatic interactions are shown as gray dotted lines. Zn1 is tetrahedrally coordinated and Zn2 is penta-coordinated. The two water molecules are labeled Wat 1 and Wat 2. **(b)** Stereoscopic view of the electron-density map in the vicinity of the active site. The coefficients $2F_o–F_c$ and calculated phases are used. The map is contoured at 1.2σ level.

on a short peptide (starting at residue 99) with the consensus sequence His-X_1-His-X_1-Asp. The two histidine residues (with the exception of the *A. hydrophilia* enzyme where the first histidine is replaced by an asparagine residue) coordinate to the tetrahedral zinc, Zn1; the invariant aspartate is a ligand of the penta-coordinated zinc, Zn2. The remaining three ligands are also invariant in all known sequences, with the exception of the enzyme from *X. maltophilia* where the cysteine ligand is replaced by an aspartate. This is a conservative replacement because a cysteine that is coordinated to zinc probably exists in the thiolate form.

The same finger print for a binuclear zinc center is found in the sequence of the *B. cereus* β-lactamase, yet the crystal structure contains only one zinc ion [26] at a position equivalent to Zn1 of the *B. fragilis* enzyme. The electron-density map around the zinc reveals a weak density, which was attributed to a water molecule. This weak density was at approximately the same position as that of the penta-coordinated zinc, Zn2, in the *B. fragilis* enzyme. The authors proposed that this is the hydrolytic water.

Equilibrium dialysis and ^{1}H NMR data for the metallo-β-lactamase from *B. cereus* [7,25], identified a large difference between the dissociation constants of the high and low affinity zinc-binding sites (2.4 μM and 24 mM). These data were obtained at low pH, pH 5.3 for the high affinity, and pH 5.7 for the low affinity sites. In addition, the solutions used in the experiments were buffered by succinate, which could chelate the low affinity zinc. These conditions could reduce zinc affinity and change the protonation states of the ligands. The crystals of the *B. cereus* enzyme were obtained at pH 5.6 in the presence of 100 μM $ZnSO_4$, much below the concentration required to saturate the second zinc-binding site. Citrate, also a chelator of zinc ions, was used to buffer the solutions. In contrast, the crystals of the *B. fragilis* enzyme were obtained at pH 7.0 and in the presence of only 10 μM $ZnCl_2$. Nevertheless, it is the binuclear zinc center that is observed in the active site, indicating that both sites are high affinity sites. The intriguing discrepancy between the two structures may be the consequence of the difference in experimental conditions, or may reflect a genuine difference in affinities. The local electrostatic environment in the active site of the *B. cereus* enzyme may result in a lower affinity for the second zinc ion to bind. One candidate for such an effect emerges when the aligned amino acid sequences of the two enzymes are analyzed in the contexts of the structure of the *B. fragilis* enzyme, and the view of the active site of the *B. cereus* enzyme provided by Carfi *et al.* [26]. Such analysis shows the second cysteine residue, Cys104, in the *B. fragilis* β-lactamase to be replaced by an arginine residue in the *B. cereus* enzyme. Cys104 is located in the vicinity of the active site, less than 6 Å away and directly underneath the metal center. Modelling shows that the longer side chain of the arginine would project towards the penta-coordinated zinc site. This would result in a profound change of electrostatics due to the positive charge of the guanidinium group. Indeed, the view of the active site presented by Carfi *et al.* [26] shows this arginine residue in close proximity to the aspartate and histidine residues, which are the ligands of the penta-coordinated zinc in the *B. fragilis* structure.

Figure 4

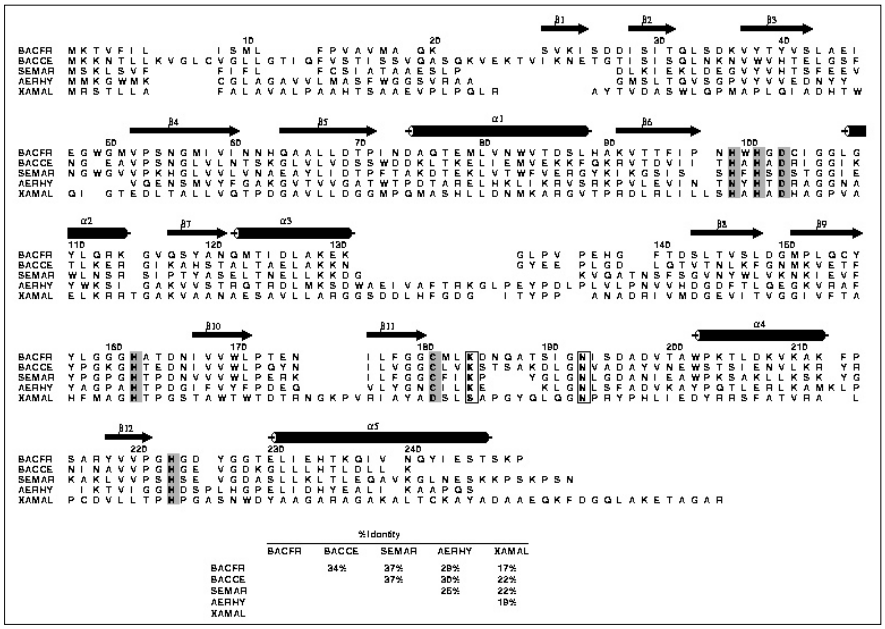

Amino acid sequence alignment of five metallo-β-lactamases. The *B. fragilis* (BACFR) and *B. cereus* (BACCE) β-lactamase sequences were aligned first. The remaining sequences from *Serratia marscescens* (SEMAR), *Aeromonas hydrophilia* (AERHY), and *Xanthomonas maltophilia* (XAMAL) were aligned against the first two using secondary structure-dependent gap penalties [73,74]. A few more changes to the automatic multiple alignment improved the conservation of the binuclear zinc fingerprint. Shaded boxes indicate zinc coordinating residues, and unshaded boxed residues are proposed to be critical for substrate binding. Secondary structure elements were assigned using DSSP and are shown above the sequence [75]. The numbering corresponds to the sequence of the *B. fragilis* enzyme. The matrix at the bottom of the figure summarizes the level of amino acid sequence identity.

Figure 5

Stereoscopic representation of the environment of Asp69, a buried aspartate residue with a sterically strained main-chain conformation. The coloring scheme is as described in the legend to Figure 3a. The sodium cation is represented as a dark purple sphere. With the exception of two water molecules, Wat1 and Wat2, all solvent molecules are internal. Zinc–ligand interactions are shown as orange dotted lines. Other key electrostatic interactions are shown as gray dotted lines.

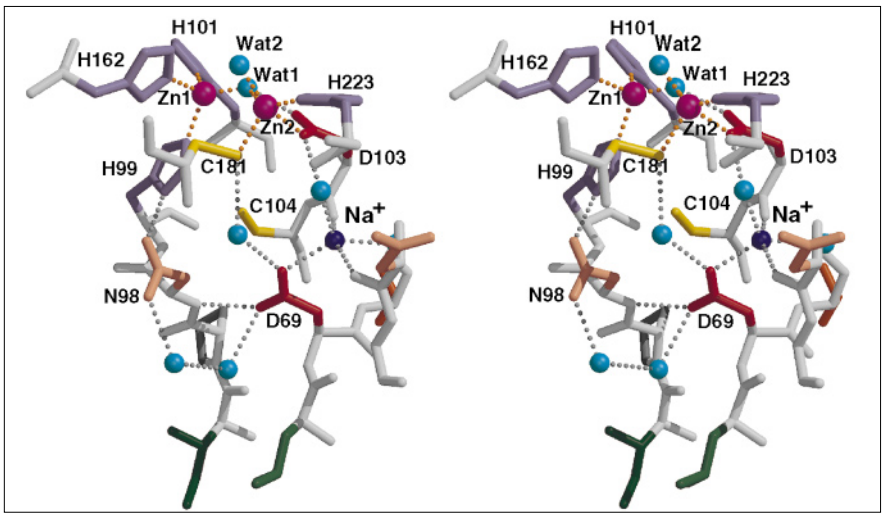

The metallo-β-lactamase from *A. hydrophila* also contains an arginine residue at position 104. This enzyme exhibits the lowest catalytic efficiency [19,20]. It remains to be determined whether the affinity for a second zinc binding correlates with the catalytic efficiencies of the various metallo-β-lactamases.

There are two more invariant amino acid residues in the active site that may stabilize the Michaelis complex and/or the the tetrahedral intermediate, Asn193 and Lys184. This is with the exception of the more remotely related enzyme from *X. maltophilia* where the lysine is replaced by a serine residue. The proposed mode of substrate binding highlights the role of these residues.

Steric strain and buried charges

Two non-glycine residues adopt sterically strained main-chain conformations: Asp69 of both molecules in the asymmetric unit, with (ϕ,ψ) dihedral angle values averaging (81°,144°), and Asp142 of molecule B in a conformation with (ϕ,ψ) values of (78°,-78°). The assigned conformations are reliable, as these residues are associated with well defined electron density and low crystallographic temperature factors. Asp69 is located at the interface between the N- and C-terminal domains of the molecule, in the vicinity of the active site, and with the carboxylate moiety buried. The main-chain conformation adopted by Asp69 is close to the left-handed helical region and helps define a 90° turn in the direction of the polypeptide chain. The turn is such that the side chain of Asp69 interacts with groups that in turn assure the disposition and orientation of three zinc ligands: His99, Cys181 and Asp103 (Fig. 5). Hence, the strained conformation of Asp69 may be relevant to the function of the enzyme. Indeed, sterically strained amino acid residues in other proteins are, on the whole, rather rare but tend to be associated with active sites [46].

The sterically strained main-chain conformation of Asp142 is observed only in molecule B. It is part of a polypeptide segment that is involved in crystal packing across the non-crystallographic twofold axis. In this context, if the non-strained conformation observed in molecule A also occurred in molecule B, it would lead to an unfavorable electrostatic interaction between the main-chain carbonyl groups of the two Asp142 residues.

There are two buried aspartate residues in the molecule and both are associated with the active site. The first, Asp69, has been discussed above, highlighting its role in positioning zinc ligands. The refined model indicates that Asp69 forms an ion pair (Fig. 5), probably with a sodium ion that was present in the crystallization solution (the HEPES buffer was titrated with NaOH). The ligands are all oxygen atoms with an average distance of 2.4 Å. The coordination geometry is trigonal bipyramidal; the sodium ion is coordinated to the carboxylate group of Asp69, to two main-chain carbonyl oxygen atoms (the apical positions), and to two water molecules. The distance between the sodium ion and the penta-coordinated zinc is 6.0 Å. It remains to be determined whether under physiological conditions this may be a magnesium or a calcium-binding site.

The second buried aspartate residue, Asp165, is also associated with positioning zinc ligands. One of the interactions of its buried carboxylate group is with the main-chain nitrogen atom of Trp100. This interaction facilitates the close proximity and the appropriate orientation of three zinc ligands: His99, His101 and His162. Asp69 is invariant in all but the metallo-β-lactamase from

Figure 6

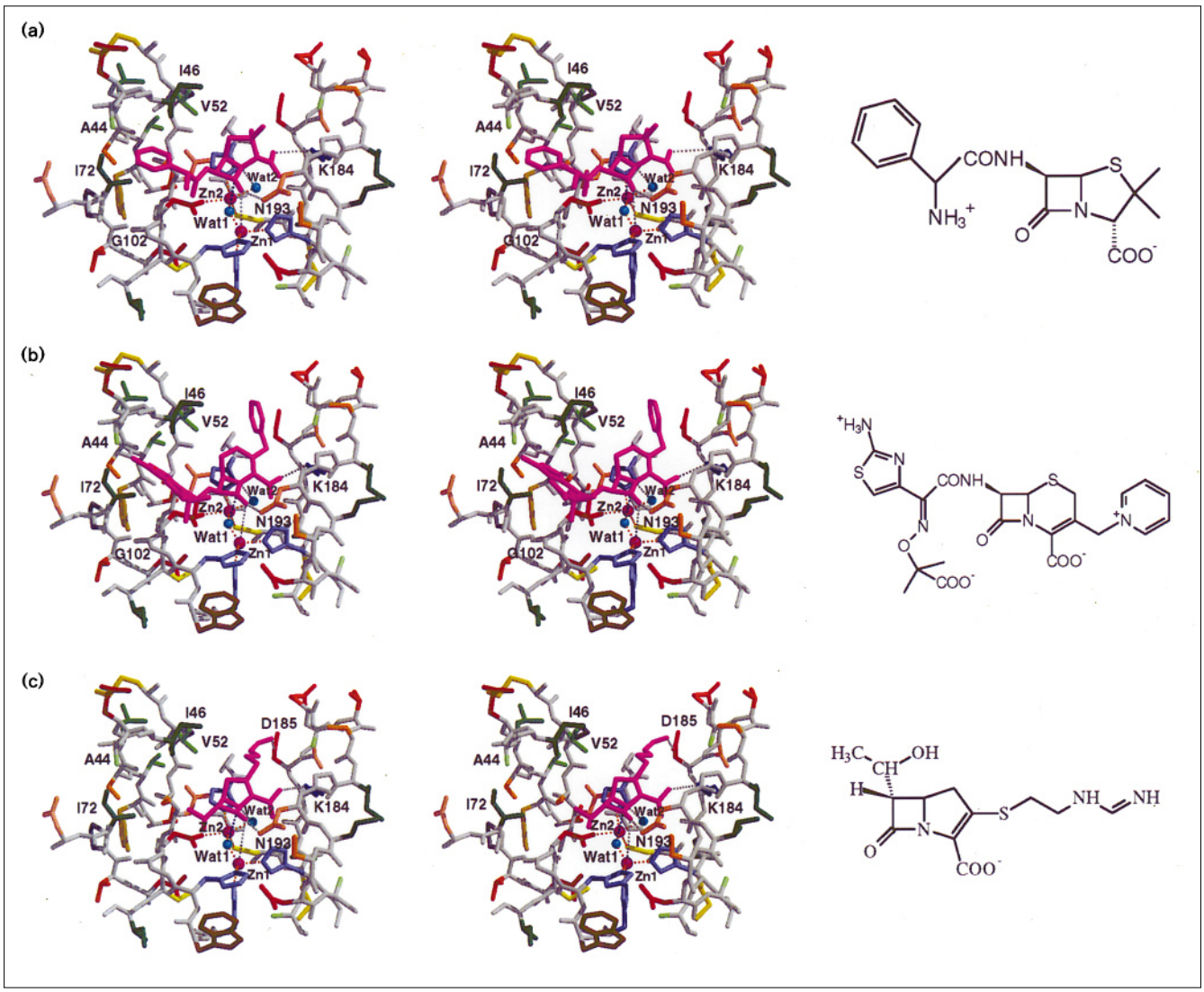

Models of β-lactam substrates bound in the active site of the metallo-β-lactamase from *B. fragilis*. The substrates, shown in magenta, are: (a) ampicillin, (b) ceftazidime and (c) imipenem. The corresponding chemical structures are displayed on the right. The coloring scheme is as described in the legend of Figure 3a. In addition, the dark blue dotted line shows the shared hydroxide's proposed line of attack on the carbonyl carbon of the substrate.

A. hydrophilia, and Asp165 is invariant in all but the enzyme from *X. maltophilia*. Where they are conserved, the two buried aspartate residues are likely to play a similar role.

Proposed mode of binding of substrates

Requirements for shape, electrostatic, and functional complementarity between the enzyme and the substrate guided the modelling of bound β-lactams in the active-site groove of the metallo-β-lactamase from *B. fragilis* (Fig. 6). Three examples of different substrates have been accommodated in the active site, without invoking major conformational adjustments of the protein. The three substrates represent different types of antibiotic that are all susceptible to the *B. fragilis* enzyme: ampicillin, a penicillin with a β side-chain substituent on the β-lactam ring; ceftazidime, a third generation cephalosporin, with a bulky β side-chain substituent; and imipenem, a penicillin with an α side-chain substituent (the enantiomorphic stereochemistry of the more commonly used β substitution). Three key assumptions help define the position and orientation of the substrate. Firstly, the nucleophilic group, which is most likely the shared hydroxide (Wat1), must be in close proximity to the β-lactam's carbonyl carbon atom. Secondly, the carboxyl moiety, common to all β-lactam substrates, forms an electrostatic interaction with the amino

group of the invariant Lys184. Thirdly, the carbonyl oxygen atom of the β-lactam bond forms an electrostatic interaction with the side chain of the invariant Asn193 and a more distant interaction with the tetrahedrally coordinated zinc, Zn1. Together, Asn193 and Zn1 provide an oxyanion hole that enhances the polarization of the β-lactam's CO bond upon binding. The oxyanion hole also stabilizes the negative charge that develops on the tetrahedral intermediate during the reaction. Indeed, in the crystal structure, a water molecule occupies the oxyanion site, indicating that a partial negative charge is favored there. The consequence of this binding mode is that the nitrogen atom of the β-lactam bond is positioned in close proximity to the apical water, Wat2. If the β-lactam model is shifted by approximately 1.5 Å the apical water could serve as the nucleophile. This pertains to the catalytic mechanism as discussed below. With the shifted models, the carboxyl moiety of the β-lactam compound forms a tighter interaction with Lys184, however, the β-lactam's carbonyl group is displaced from the oxyanion hole.

A hydrophobic pocket, formed by the side chains of Ala44, Ile46, Val52 and Ile72, complements the aromatic tip of the β side-chain substituents of ampicillin and ceftazidime. In the models shown in Figures 6a,b, the side chain has been adjusted to occupy the hydrophobic pocket and to orient the peptide's carbonyl group towards the main-chain amide groups of Gly102 and Asp103. Other combinations of side-chain dihedral angles can be selected, in which the peptide is oriented away from the above two amides but the aromatic group still occupies the hydrophobic pocket. Residues 45–51 that delineate part of the hydrophobic pocket are associated with high crystallographic temperature factors (with residues 48–49 being completely disordered) and comprise the end of a hairpin loop that protrudes into the solvent (Figs 1,2,3). Conceivably, this 'flap' may adjust upon substrate binding to accommodate a variety of β-lactam side-chain substituents.

For imipenem (Fig. 6c), the short α side-chain group can not occupy the hydrophobic pocket. However, there is enough space to accommodate this substrate even though an α substitution results in a side chain that is oriented towards the floor of the active site groove. Enhancement of the binding energy may be provided by interactions between the protein and the long side-chain substituent attached to the five-membered thiazolidine ring, and projecting along the narrow groove. In the model, the conformation of this thiazolidine ring substituent has been adjusted to form an electrostatic interaction with Asp185, but as this is not an invariant residue, other interactions may be involved.

The active-site groove is open at both ends (Fig. 2), and can accommodate the large side-chain substituents of the fused six-membered ring typical of cephalosporins. These substituents form good leaving groups during cephalosporin hydrolysis. The kinetic data for the *B. cereus* enzyme indicated that the rate limiting step in hydrolysis is the formation of the tetrahedral intermediate, rather than the release of the leaving group [47]. Structurally, having an open groove enables the leaving groups to diffuse away from the active site.

With the models of bound substrates in mind, the wide spectrum substrate profile of the metallo-β-lactamase from *B. fragilis* is attributed to a combination of structural features. Firstly, when the shape and size of the active site is compared with that of a class A β-lactamase [48] it is obvious that the active site of the metallo-β-lactamase is wider and less restrictive. This less restrictive site thus allows more latitude in accommodating substrates of varying size and shape. For example, a model of imipenem cannot be accommodated in the active site of the class A β-lactamase because its side chain substituent is sterically hindered. Secondly, the inherent flexibility of the β hairpin loop, in the *B. fragilis* enzyme (residues 44–51), may help compliment a wide variety of β-lactam side-chain substituents.

The mode of binding presented here bears little resemblance to that sketched by Carfi *et al.* [26]. Their model of bound cephalosporin implies that while the carbonyl oxygen atom of the β-lactam ring interacts with the tetrahedral zinc, and the carboxylate moiety forms a salt bridge with His210 (His223 in the numbering scheme of the *B. fragilis* enzyme), a nucleophilic attack on the β-lactam ring is possible by the water molecule that interacts with Asp90 (Asp103 in the current numbering scheme). This is the water molecule located at the approximate position of the penta-coordinated zinc in the *B. fragilis* enzyme. In our hands, the orientation and the position of the substrate cannot be reconciled in this manner, with either a water replacing the penta-coordinated zinc or with the shared hydroxide (Wat1) being assigned with the nucleophilic role.

The catalytic mechanism

The most attractive candidate to carry out the nucleophilic attack on the carbonyl carbon of the β-lactam ring is the shared hydroxide. Its interaction with Asp103 helps orient the lone pair electrons for a *re*-face attack on the β-lactam, and also modulates the strength of the hydroxide-zinc interaction, so that the hydroxide is not too tightly bound. This arrangement is reminiscent of other hydrolases with a binuclear metal center, for example urease, with a binuclear nickel center [49] and phosphotriesterase, with a binuclear cadmium center [40]. In these proteins a solvent molecule which bridges the two metals ions, and is postulated to exist predominantly in the form of a hydroxide, is the proposed nucleophile. In β-lactamase an aspartate residue coordinates via one carboxylate oxygen atom to one of the metal ions, and simultaneously forms an

Table 2

Kinetic parameters for the hydrolysis of benzylpenicillin by *B. fragilis* zinc β-lactamase.

pH	k_{cat} (s^{-1})	K_m (μM)	k_{cat}/K_m ($\mu M^{-1}s^{-1}$)
5.0	332	180.0	1.8
6.0	290	63.8	4.5
7.0	247	23.7	10.4
8.0	277	18.3	15.1

electrostatic interaction with the hydroxide via the second carboxylate oxygen atom.

By analogy with either single or binuclear metallo-hydrolases, the nucleophilic attack results in a negatively-charged tetrahedral intermediate. Stabilization of this state is provided by the oxyanion hole. The next step in the reaction requires a proton to be transferred to the amide nitrogen of the β-lactam bond. With the binuclear zinc center of β-lactamase, the apical water, Wat2, is optimally positioned to donate a proton (Fig. 6). Whether or not the proton transfer is the rate limiting step is yet to be determined. Once Wat2 is converted into a hydroxide, it can readily move to occupy the vacated Wat1 site, as the tetrahedral intermediate state decomposes and the degraded β-lactam diffuses away from the active site. Finally, a water molecule from the bulk solvent will re-occupy the apical coordination site of the penta-coordinated zinc.

A catalytic mechanism which invokes the apical water molecule as the nucleophilic group and the shared hydroxide as playing more of a structural role, by maintaining the integrity of the zinc cluster, should not be ignored. Models of bound substrates consistent with such a mechanism can be derived. In favor of this model, it may be argued that the apical water would be less tightly bound compared with the shared hydroxide, and therefore might constitute a better nucleophilic group. The inherent weaknesses of the proposal are that there are no protein groups that are appropriately positioned to assist with the proton transfer, and the tetrahedral intermediate cannot be stabilized by the oxyanion hole. Thus, although this alternative catalytic mechanism cannot currently be ruled out, it is less favored.

The pH dependence of the observed k_{cat} values remains relatively constant between the range pH 5–8 (Table 2). This is consistent with the interpretation that the interaction with the two zinc ions dramatically reduces the pK_a of the shared hydroxide. This trend of pH dependence is quite different from the distorted bell-shaped curve observed with the single zinc-bound form of the enzyme from *B. cereus* [50]. For the *B. cereus* enzyme, the drop in the catalytic rate at low pH implicated a group with a pK_a value of 5.1 for the substrate-bound state. On the other hand, the observed K_m of the *B. fragilis* β-lactamase increases ten-fold as the pH is reduced from 8 to 5, whereas the increase is only twofold for the *B. cereus* enzyme. The *B. fragilis* β-lactamase data can be reconciled by a kinetic model in which an ionizable group, presumably the shared hydroxide, has a pK_a value of 6.2 in the free form of the enzyme. The pKa value is further reduced to 4.2 upon substrate binding. Indeed, it makes sense that upon desolvation of the active site by the substrate the protonation of the hydroxide is less favorable because the negative charge is required to compliment the charges of the two buried zinc ions.

Could the *B. fragilis* metallo-β-lactamase function with a single metal ion? By analogy with the crystal structure of the *B. cereus* enzyme, if only one zinc ion was present it would occupy the tetrahedral zinc site. The substrates would bind in a mode not much different than that proposed for the binuclear zinc center form. The nucleophilic water molecule would be located approximately half way between the positions of the hydroxide and the penta-coordinated zinc, forming electrostatic interactions with Asp103 and His223. These two residues would provide the assisting machinery for proton transfer. An evolutionary progress towards an enzyme with a binuclear center may be invoked because, with Asp103 and His223 in position to fulfill their role, most of the elements for binding a second zinc ion are already in place. The third ligand may be a cysteine or an aspartate residue, or even just a water molecule. The elimination of any positively charged side chain proximal to the metal site is also required. The binuclear cluster may provide bacteria with an evolutionary advantage, by assuring that the hydrolytic water is always in an anionic form and that there is a readily available second water to provide the proton. This hypothesis may be simply tested by replacing Arg104 (*B. fragilis* numbering scheme) of the metallo-β-lactamase from *B. cereus* by a cysteine residue and evaluating the kinetic properties of the engineered enzyme. Alternatively, the *B. fragilis* enzyme could be converted into an enzyme with a second low affinity zinc-binding site.

Biological implications

The production of β-lactamases by pathogenic bacteria has greatly diminished the usefulness of β-lactam antibiotics. The increasing number of metallo-β-lactamases that have been identified in recent years raises further concern about the effectiveness of one of the most powerful families of therapeutic agents. The resistance of *B. fragilis* to β-lactams, conferred by the metallo-β-lactamase, is particularly alarming because this pathogen is associated with post-surgery infections. Moreover, the enzyme exhibits a broad-spectrum substrate profile and is not clinically susceptible to any known β-lactamase inhibitor. The report of plasmid-mediated dissemination of the enzyme indicates future acceleration of acquired

resistance to β-lactams by related bacteria. The crystal structure determination of the enzyme was undertaken to gain insight into the catalytic mechanism and to assist with the drug design effort.

Despite the similarity in fold and disposition of active-site residues, the metallo-β-lactamase from *B. fragilis* was found to contain a binuclear zinc center, whereas the enzyme from *B. cereus* contains only a single zinc ion. This surprising finding is intriguing in terms of the evolution of the active sites. The current work provides the structural basis for understanding the differences that may have led to the lower zinc-binding affinity to the potential penta-coordinated site in the *B. cereus* enzyme. This study also reveals that the fingerprint for the binuclear zinc center is conserved in all the metallo-β-lactamases of known sequence. Whether the catalytic efficiency of each of the metallo-β-lactamases correlates with the affinity to the second zinc ion is not yet known.

A new model for bound substrate is proposed, implying that a hydroxide group, that coordinates to both zinc ions, serves as the nucleophilic group; the proton is provided by a water molecule that coordinates to the penta-coordinated zinc. In addition to the invariant residues that are required for metal binding, two more invariant residues are implicated in function. The first of these is an asparagine residue the side chain of which, together with the tetrahedral zinc ion, forms an oxyanion hole. The second residue is a lysine whose amino group compliments the charge of the carboxylate moiety, typical of all β-lactam antibiotics. The broad-spectrum substrate profile of metallo-β-lactamase arises from the rather wide groove where β-lactam compounds of various size and shape can be accommodated. In addition, the flexibility of a β hairpin loop associated with the active site indicates that it may adopt its conformation to complement a variety of β-lactam side-chain substituents.

Materials and methods

Crystallization and data collection

The *CcrA3* gene of the metallo-β-lactamase from *B. fragilis* (isolated at Queen's Medical College, London [QMCN3]) was cloned and over-expressed in *E. coli*. The protein was purified as described previously [16,21]. The polypeptide chain consists of amino acids 18–249 with a molecular mass of approximately 26 kDa [16]. The signal sequence comprising residues 1–17 has been omitted from the cloned gene. Single crystals of the Zn^{2+}-bound β-lactamase have been obtained at room temperature by vapor diffusion in hanging drops. The protein drops were prepared by mixing 5 µl of 5–8 mg ml^{-1} protein solution (in 10 mM HEPES, pH 7.0, and 10 µM $ZnCl_2$) with 5 µl of reservoir solution containing 26–28% PEG 2000, buffered at pH 7.0 by 0.1 M HEPES. The drops were equilibrated against 500 µl of reservoir solution for 1–2 weeks, after which the crystals reached a maximum size of 0.25 x 0.25 x 0.6 mm^3. The crystals belong to the tetragonal space group $P4_32_12$ with unit cell dimensions a=b=78.3 Å, c=140.9 Å. There are two molecules in the asymmetric unit, and the solvent constitutes 40% of the cell.

The crystals are very sensitive to X-rays and to avoid radiation damage cryocrystallographic techniques have been employed for all data collection, using glycerol as the cryoprotectant. The crystals were transferred into 10 µl dialysis buttons, and dialyzed for 4–48 h against a solution containing 30% PEG 2000, 0.1 M HEPES at pH 7.0, and 18% glycerol. The crystals were transferred into a nylon fiber loop (Ethilon 10-0 ophthalmic 0.2 m) glued to a glass capillary tube [51]. Flash-freezing of the crystals to approximately 120K was achieved with a modified Enraf-Nonius FR558 liquid nitrogen cryostat. X-ray diffraction data from the native crystals and crystals soaked with heavy-atom derivative solutions were collected in-house using a Siemens multi-wire area detector mounted on a three-circle goniostat. Monochromated CuK^{α} X-rays were supplied by a Rigaku R200BH rotating-anode generator operating at 100 mA x 40 kV. Oscillation steps of 0.20° or 0.25° were sampled about the goniostat's ω-axis, using crystals whose mosaic spread were typically 0.7–0.8°. The freezing did not alter the unit cell dimensions significantly.

The data were processed using the XENGEN computer package [52]. Native data were collected at 1.85 Å resolution (Table 3). Of the numerous heavy-atom derivative replacement experiments only two produced interpretable diffraction changes: $CdCl_2$, which was obtained from a protein sample that was renatured in the presence of the cation; and K_2HgI_4/KI, which was soaked into the crystal. The data were useful only at low resolution and the resulting electron-density map was uninterpretable.

Multiwavelength anomalous diffraction (MAD) data [53,54] were collected from a native, Zn^{2+}-bound protein crystal, exploiting the K absorption edge of the intrinsic zinc (1.238 Å, 9.66 keV). The MAD data were collected at the X12C beamline of the National Synchrotron Light Source (Brookhaven National Laboratory, Upton, NY). All data were obtained from a single crystal that was flash-frozen using the Oxford Cryosystem. The crystal revealed an unexpectedly strong fluorescence X-ray absorption near-edge structure signal, which in retrospect is attributed to the close association of two zinc ions (Fig. 7). Diffraction intensities to 2.0 Å resolution were recorded on a 300 mm MAR research image plate, sampling oscillation steps of 1.0°, and using the inverse-beam strategy (rotation of the crystal by 180° to

Figure 7

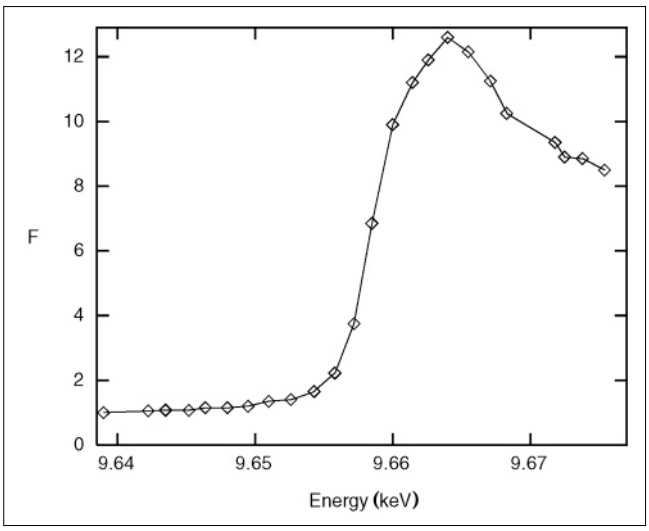

Fluorescence X-ray absorption spectrum of the single crystal of zinc β-lactamase from *B. fragilis* used for data collection. X-ray diffraction data were collected at nominal incident X-ray energies of 9.6575 (λ1), 9.6637 (λ2) and 9.9188 (λ3) keV. F is measured in arbitrary units.

Table 3

Data processing statistics for the native data set.

Shell lower limit (Å)	No. of reflections Possible	Collected	No. of observations	⟨I/σ(I)⟩	R_{sym}*
3.36	6693	6671	69 777	49.3	0.050
2.67	6409	6409	67 124	22.4	0.081
2.33	6324	6324	48 345	9.7	0.143
2.12	6274	6274	42 663	6.4	0.196
1.97	6252	6232	37 170	3.9	0.274
1.85	6257	5995	27 319	1.7	0.398
Total	38 209	37 905	292 398	16.1	0.077

*$R_{sym} = \Sigma_{i,(hkl)}|I_{i,(hkl)} - \langle I_{(hkl)}\rangle|/\Sigma_{i,(hkl)}\langle I_{(hkl)}\rangle$, where $\langle I_{(hkl)}\rangle$ is the average intensity of symmetry equivalent reflections.

obtain the Bijvoet pairs). Data acquisition was controlled with the computer program MADNES [55], driven by a graphical user interface (R M Sweet, J Skinner, [abstract 1a.7.A.], American Crystallographic Association Annual Meeting, Montreal, Canada, 1995). Measurements were taken at three wavelengths corresponding to the zinc's K absorption edge inflection point (λ1=1.2830 Å), peak (λ2=1.2838 Å), and a remote high-energy point (λ3=1.2500 Å). The intensity data were processed with the DENZO/SCALEPACK computer programs [56]. The statistics of data collection are shown in Table 4.

Structure determination

The multiwavelength data were treated as arising from MIR experiments following protocols described previously [57,58]. The data measured at wavelength λ1 were chosen as the 'native' set, while the data sets at λ2 and λ3 were treated as 'derivatives with anomalous scattering'. The anomalous differences $\Delta F+/-(\lambda 2)$ were used in SHELXS-90 to calculate the difference anomalous Patterson function, which was interpreted by the Patterson superposition minimum function method [59]. The analysis showed unambiguously that there are four zinc sites in the asymmetric unit, corresponding to each β-lactamase molecule binding two Zn^{2+}, 3.5 Å apart. The CCP4 suit of programs [60] was used to prepare the data for phasing. The positions, isotropic temperature factors, and the dispersive and anomalous occupancies of the four zinc scatterers in the asymmetric unit were refined at 2.4 Å resolution using the program MLPHARE [61] as implemented in CCP4. The four sites refined with approximately the same occupancy values (Table 5). Cross-difference Fourier maps of the mercury and the cadmium derivatives, calculated with phases generated by the MAD experiment, confirmed that the space group is $P4_32_12$ and not $P4_12_12$. The MAD-phased electron-density map at 2.4 Å resolution was readily interpretable. The phases were further improved by solvent flattening techniques [62] as implemented in the computer program DM [63], and by applying non-crystallographic averaging using the computer program RAVE [64,65]. All three maps (i.e. the MAD-phased map, the solvent-flattened map, and the averaged map) were used to trace the polypeptide chain using the interactive computer graphics program O [66] running on a Silicon Graphics INDIGO 2 workstation.

Structure refinement

The computer program package X-PLOR [67] was used to refine the structure (Table 6). The initial model included most of the amino acid residues and the zinc ions. The model was refined against the 1.85 Å diffraction data collected on the Siemens area detector. The progress of the refinement was evaluated from the improved quality of the electron-density maps and the values of the conventional R and R_{free} [68]. The improvement of the electron-density maps enabled the tracing of all but a few residues. The first cycle of refinement included a slow-cooling step in the range 3000 K to 300 K, followed by positional refinement and by individual temperature factor refinement. Electron-density maps with the coefficients $2|F_o|-|F_c|$ and $|F_o|-|F_c|$ and calculated phases were used to adjust the model on the interactive graphics system. At the early stages of refinement non-crystallographic symmetry restraints were applied, but later, the two molecules in the asymmetric units were refined independently. Charged residues and sodium and zinc ions were refined as neutral, and no restraints were applied between the zinc ions and their ligands. Solvent molecules were assigned by a peak search of the difference Fourier map. The cut-off level for inclusion in the model was 3.5σ of the rms density. During the last four rounds of positional refinement, the 10% of the reflections

Table 4

Data processing statistics for the MAD data set.

Data set	λ (Å)	Maximum resolution (Å)	R_{sym}*	Completeness (%)	Redundancy*
λ1	1.28386	2.0	0.039 (0.043)	79.8	6.6 (12.3)
λ2	1.28306	2.0	0.041 (0.060)	92.6	5.6 (10.3)
λ3	1.25000	2.0	0.039 (0.047)	79.7	6.6 (12.2)

*$R_{sym} = \Sigma_{i,(hkl)}|I_{i,(hkl)} - \langle I_{(hkl)}\rangle|/\Sigma_{i,(hkl)}\langle I_{(hkl)}\rangle$, where $\langle I_{(hkl)}\rangle$ is the average intensity of symmetry equivalent reflections. R_{sym} values correspond to unmerged Bijvoets pairs. R_{sym} values for merged Bijvoets pairs are listed in parentheses. Similarly, the redundancy values correspond to unmerged and merged Bijvoets pairs.

Table 5

Refinement of anomalous scatterer sites.

	Site No.	Occupancy Real	Occupancy Anomalous	B factor
λ2	1	3.9	6.8	17.4
	2	3.4	5.6	13.9
	3	4.5	6.5	17.2
	4	3.7	5.5	16.6
λ3	1	8.7	4.2	17.3
	2	8.8	4.4	14.9
	3	9.0	4.1	18.8
	4	9.0	4.4	17.3

Mean figure of merit = 0.62; λ2 and λ3 are as in Table 3.

previously used for the calculation of the R_{free} values were included in the refinement, and the energy minimization was applied without electrostatic terms.

Enzyme kinetics

Kinetic measurements were made on a Gilford 250 spectrophotometer, using freshly prepared benzylpenicillin (extinction coefficient $\Delta\varepsilon_{240}$=540 $M^{-1}cm^{-1}$). All assays were performed at 25°C in 50 mM phosphate buffer. The concentration of Zn^{2+} in the protein solution was 10 μM. Initial steady-state rates were obtained at 6–7 substrate concentrations. Experiments spanned the pH range 5–8. The data were analyzed with the computer program ENZPACK (Elsevier).

Accession number

The atomic coordinates have been deposited in the Brookhaven Protein Data Bank with the accession code 1ZNB.

Table 6

Refinement statistics.

Resolution range (Å)	8.0–1.85
No. unique reflections, F >2σ(F)	34 597
Completeness (%)	
overall (8.0–1.85 Å)	91.9
1.92–1.85 Å shell	73.6
R	0.167
R_{free}*	0.241
Number of atoms in the asymmetric unit	
protein	3540
solvent	529
Zn^{2+}	4
rms deviations from ideal geometry	
bond length (Å)	0.02
bond angle (°)	1.9
Average B factors (Å^2)	
protein main chain	15
protein side chain	17
solvent molecules	31
metal ions	12

*The R value is for 10% of the reflection, randomly selected, that were not included in the refinement.

Acknowledgements

We are grateful to Drs Robert Sweet, John Skinner, and Mr Salvatore Sclafani at the National Synchrotron Light Source (Brookhaven National Laboratory, Upton, NY) for their generous help and advice in data collection and data processing. We thank Drs Ursula Pieper and Laura Zawadzke for sharing the load of data collection in Brookhaven. The stimulating discussions about the mechanism with Drs Morris Krauss and Walter Stevens, and the help from Dr Michael Gilson in the interpretation of the kinetic data are much appreciated. This work was funded by American Cyanamid Medical Research Division.

References

1. Frère, J.-M. & Joris, B. (1985). Penicillin-sensitive enzymes in peptidoglycan biosynthesis. *Crit. Rev. Microbiol.* **11**, 299–396.
2. Abraham, E.P. & Chain, E. (1940). An enzyme from bacteria able to destroy penicillin. *Nature* **146**, 837.
3. Ambler, R.P. (1980). The nature of β-lactamases. *Philos. Trans. R. Soc. Lond.* [Biol.] **289**, 321–331.
4. Jaurin, B. & Grundström, T. (1981). *AmpC* cephalosporinase of *Escherichia coli* K-12 has a different evolutionary origin from that of β-lactamases of the penicillinase type. *Proc. Natl. Acad. Sci. USA* **78**, 4897–4901.
5. Houvinen, P., Houvinen, S. & Jacoby, G.A. (1988). Sequence of PSE-2 β-lactamase. *Antimicrob. Agents Chemother.* **32**, 134–136.
6. Sabath, L.D. & Abraham, E.P. (1966). Zinc as cofactor for cephalosporinase from *Bacillus cereus* 569. *Biochem. J.* **98**, 11–13.
7. Davies, R.B. & Abraham, E.P. (1974). Metal cofactor requirements of β-lactamase II. *Biochem. J.* **143**, 129–135.
8. Ambler, R.P., Daniel, M., Fleming, J., Hermoso, J.M., Pang, C. & Waley, S.G. (1985). The amino acid sequence of the zinc-requiring β-lactamase II from the bacterium *Bacillus cereus* 569. *FEBS Lett.* **189**, 207–211.
9. Thompson, J.S. & Malamy, M.H. (1990). Sequencing the gene for an imipenem-cefoxitin-hydrolyzing enzyme (CfiA) from *Bacteroides fragilis* TAL2480 reveals strong similarity between CfiA and *Bacillus cereus* β-lactamase II. *J. Bacteriol.* **172**, 2584–2593.
10. Rasmussen, B.A., Guzman, Y. & Tally, F.P. (1990). Cloning and sequencing of the class B β-lactamase gene (*ccrA*) from *Bacteroides fragilis* TAL3636. *Antimicrob. Agents Chemother.* **34**, 1590–1592.
11. Massidda, O., Rossolini, G.M. & Satta, G. (1991). The *Areomonas hydrophilia* cphA gene: molecular heterogeneity among class B metallo-beta-lactamases. *J. Bacteriol.* **173**, 4611–4617.
12. Segatore, B., Massida, O., Satta, D. & Amicosante, G. (1993). High specificity of cphA-encoded metallo-beta-lactamase from *Aeromonas hydrophila* AE036 for carbapenems and its contribution to β-lactam resistance. *Antimicrob. Agents Chemother.* **37**, 1324–1328.
13. Walsh, T.R., *et al*,. & Bennet, P.M. (1994). Sequence analysis of the L1 metallo-beta-lactamase from *Xanthomonas maltophilia. Biochim. Biophys. Acta* **1218**, 199–201.
14. Osano, E., *et al*., & Kato, N. (1994). Molecular characterization of an enterobacterial metallo β-lactamase found in clinical isolate of *Serratia marscescens* that shows imipenem resistance. *Antimicrob. Agents Chemother.* **38**, 71–78.
15. Bandoh, K., Muto, Y., Watanabe, K., Katoh, N. & Ueno, K. (1991). Biochemical properties and purification of metallo-β-lactamase from *Bacteroides fragilis. Antimicrob. Agents Chemother.* **35**, 371–372.
16. Yang, Y., Rasmussen, B.A. & Bush, K. (1992). Biochemical characterization of the metallo-β-lactamase CcrA from *Bacteroides fragilis* TAL3636. *Antimicrob. Agents Chemother.* **36**, 1155–1157.
17. Mathews, B.W. (1988). Structural basis of the action of thermolysin and related zinc peptidases. *Acc. Chem. Res.* **21**, 333–340.
18. Christianson, D.W. & Lipscomb, W.N. (1989). Carboxypeptidase A. *Accounts. Chem. Res.* **22**, 62–69.
19. Felici, A., *et al*., & Frère, J.-M. (1993). An overview of the kinetic parameters of class B β-lactamases. *Biochem. J.* **291**, 151–155.
20. Felici, A. & Amicosante, G. (1995). Kinetic analysis of extension of substrate specificity with *Xanthomonas maltophilia, Aeromonas hydrophila*, and *Bacillus cereus* metallo-β-lactamases. *Antimicrob. Agents Chemother.* **39**, 192–199.
21. Rasmussen, B.A., Yang, Y., Jacobus, N. & Bush, K. (1994). Contribution of enzymatic properties, cell permeability, and enzyme expression to microbiological activities of β-lactams in three *Bacteroides fragilis* isolates that harbor a metallo-β-lactamase gene. *Antimicrob. Agents Chemother.* **38**, 2116–2120.
22. Marumo, K., Takeda, A., Nakamura, Y. & Nakaya, K. (1995). Purification and characterization of metallo-β-lactamase from *Serratia marcescens*. *Microbiol. Immunol.* **39**, 27–33.

23. Paton, R., Miles, R.S. & Amyes, S.G.B. (1994). Biochemical properties of inducible β-lactamases produced from *Xanthomonas maltophilia*. *Antimicrob. Agents Chemother*. **38**, 2143–2149.
24. Bush, K., Macalintal, C., Rasmussen, B.A., Lee, V.J. & Yang, Y. (1993). Kinetic interactions of tazobactam with β-lactamases from all major structural classes. *Antimicrob. Agents Chemother*. **37**, 851–858.
25. Baldwin, G.S., Galdes, A., Hill, A.O., Smith, B.E., Waley, S.G. & Abraham, E.P. (1978). Histidines residues as zinc ligands in β-lactamase II. *Biochem. J.* **175**, 441–447.
26. Carfi, A., *et al*., & Dideberg, O. (1995). The 3-D structure of a zinc metallo-β-lactamase from *Bacillus cereus* reveals a new type of protein fold. *EMBO J.* **14**, 4919–4921.
27. Rasmussen, B.A. & Bush, K. (1996). Carbapenem-hydrolyzing β-lactamases. *Antimicrob. Agents Chemother*, in press.
28. Brook, I. (1989). Pathogenicity of the *Bacteroides fragilis* group. *Ann. Clin. Lab. Sci.* **19**, 360–376.
29. Nord, C.-E., Olsson, B. & Dornbusch, K. (1978). β-lactamases in *Bacteroides*. *Scand. J. Infect. Dis. Suppl*. **13**, 27–32.
30. Rasmussen, B.A., Bush, K. & Tally, F.P. (1993). Antimicrobial resistance in *Bacteroides*. *Clin. Infect. Dis.* **16**, 390–400.
31. Hecht, D.W. & Malamy, M.H. (1989). Tn4399, a conjugal mobilizing transposon of *Bacteroides fragilis*. *J. Bacteriol*. **171**, 3603–3608.
32. Read, R.J. (1986). Improved Fourier coefficients for maps using phases from partial structures with errors. *Acta Cryst*. A **42**, 140–149.
33. Engh, R.A. & Huber, R. (1991). Accurate bond and angle parameters for X-ray protein structure refinement. *Acta Cryst*. A **47**, 392–400.
34. Kabsch, W. (1976). A solution for the best rotation to relate two sets of vectors. *Acta Cryst*. A **32**, 922–923.
35. Oefner, C. & Suck, D.J. (1986). Crystallographic refinement and structure of DNase I at 2 Å resolution. *J. Mol. Biol*. **192**, 605–632.
36. Mol, C.D., Kuo, C.-F., Thayer, M.M., Cunningham, R.P. & Tainer, J.A. (1995). Structure and function of the multifunctional DNA-repair enzyme exonuclease III. *Nature* **374**, 381–386.
37. Brannigan, J.A., *et al*., & Murzin, A.G. (1995). A protein catalytic framework with an N-terminal nucleophile is capable of self activation. *Nature* **378**, 416–419.
38. Vallee, B.L. & Auld, D.S. (1993). New perspective on zinc biochemistry: cocatalytic sites in multi-zinc enzymes. *Biochemistry* **32**, 6493–6500.
39. Kim, E.E. & Wyckoff, H.W.J. (1991). Reaction mechanism of alkaline phosphatase based on crystal structures. *J. Mol. Biol.* **218**, 449–464.
40. Benning, M.M., Kuo, J.M., Raushel, F.M. & Holden, H.M. (1995). Three-dimensional structure of the binuclear metal center of phosphotriesterase. *Biochemistry* **34**, 7973–7978.
41. Beese, L.R. & Steitz, T.A. (1991). Structural basis for the 3′ – 5′ exonuclease activity of *Escherichia coli* DNA polymerase I: a two metal ion mechanism. *EMBO J.* **10**, 25–33.
42. Volveda, A., Lahm, A., Sakiyama, F. & Suck, D. (1991). Crystal structure of *Penicillium citrinum* P1 nuclease at 2.8 Å resolution. *EMBO J.* **10**, 1607–1618.
43. Hough, E., *et al.,* & Derewenda, Z. (1989). High-resolution (1.5 Å) crystal structure of phospholipase C from *Bacillus cereus*. *Nature* **338**, 357–360.
44. Chervier, B., Schalk, C., D'Orchymony, H., Rondeau, J.-M., Moras, D. & Tarnus, C. (1994). Crystal structure of *Aeromonas proteolytica* aminopeptidase: a prototypical member of the co-catalytic zinc enzyme family. *Structure* **2**, 283–291.
45. Burley, S.K., David, P.R., Sweet, R.M., Taylor, A. & Lipscomb, W.N. (1992). Structure determination and refinement of bovine lens leucine aminopeptidase and its complex with bestatin. *J. Mol. Biol*. **224**, 113–140.
46. Herzberg, O. & Moult, J. (1991). Analysis of steric strain in the polypeptide backbone of protein molecules. *Proteins* **11**, 223–229.
47. Buckwell, S.C., Page, M.I., Longridge, J.L. & Waley, S. (1988). Hydrolysis of 3-substituted cephalosporins catalysed by β-lactamases I and II from *Bacillus cereus* and hydroxide ion. *J. Chem. Soc. Perkin Trans*. II, 1823–1827.
48. Herzberg, O. & Moult, J. (1987). Bacterial resistance to β-lactam antibiotics: crystal structure of β-lactamase from *Staphylococcus aureus* PC1 at 2.5 Å resolution. *Science* **236**, 694–701.
49. Jabri, E., Carr, M.B., Hausinger, R.P. & Karplus, P.A. (1995). The crystal structure of urease from *Klebsiella aerogenes*. *Science* **268**, 998–1004.
50. Bicknell, R., Knott-Hunziker, V. & Waley, S. (1983). The pH-dependence of class B and class C β-lactamases. *Biochem. J.* **213**, 61–66.
51. Teng, T.-Y. (1990). Mounting of crystals for macromolecular crystallography in a free-standing thin film. *J. Appl. Cryst.* **23**, 387–391.
52. Howard, A.J., Gililand, G.L., Finzel, B.C., Poulos, T., Ohlendorf, D.O. & Saleme, F.R. (1987). The use of an imaging proportional counter in macromolecular crystallography. *J. Appl. Cryst.* **20**, 383–387.
53. Hendrickson, W.A. (1991). Determination of macromolecular structures from anomalous diffraction of synchrotron radiation. *Science* **254**, 51–58.
54. Smith, J.L. (1991). Determination of three-dimensional structure by multiwavelength anomalous diffraction. *Curr. Opin. Struct. Biol.* **1**, 1002–1011.
55. Messerschmidt, A. & Pflugrath, J.W. (1987). Crystal orientation and X-ray pattern prediction routines for area detector diffractometer systems in macromolecular crystallography. *J. Appl. Cryst.* **20**, 306–315.
56. Otwinowsky, Z. (1993). Oscillation Data Reduction Program. In *Data Collection and Processing*, *Proceedings of the CCP4 Study Weekend.* (Sawyer, L., Isaacs, N. & Bailey, S., eds), pp. 56–62, SERC, Daresbury Laboratory, Warrington, UK.
57. Ramakrishnan, V., Finch, J.T., Graziano, V., Lee, P.L. & Sweet, R.M. (1993). Crystal structure of globular domain of histone H5 and its implications for nucleosome binding. *Nature* **362**, 219–223.
58. Glover, I.D., *et al*., & Tame, J.R.H. (1995). Structure determination of OppA at 2.3 Å resolution using multi-wavelength anomalous dispersion methods. *Acta Cryst.* D **51**, 39–47.
59. Sheldrick, G.H. (1991). Heavy atom location using SHELXS-90. In *Isomorphous Replacement and Anomalous Scattering*, Proceedings of the CCP4 Study Weekend. (Wolf, W., Evans, P.R. & Leslie, A.G.W., eds), pp. 23–38, SERC, Daresbury Laboratory, Warrington, UK.
60. Collaborative Computational Project No. 4. (1979). *The CCP4 Suite: Programs for Protein Crystallography*. *Acta Cryst*. D **50**, 760–763.
61. Otwinowski, Z. (1991). Maximum likelihood refinement of heavy atom parameters. In *Isomorphous Replacement and Anomalous Scattering*, Proceedings of the CCP4 Study Weekend. (Wolf, W., Evans, P.R. & Leslie, A.G.W., eds), pp. 80–86, Daresbury Laboratory, Warrington, UK.
62. Wang, B.-C. (1985). Resolution of phase ambiguity in macromolecular crystallography. *Methods Enzymol.* **115**, 90–112.
63. Cowtan, K. (1994). 'dm': an automated procedure for phase improvement by density modification. *Joint CCP4 and ESF-EACBM Newsletter on Protein Crystallography.* **31**, pp. 34–38.
64. Jones, T.A. (1992). a, yaap, asap, @#*? A set of averaging programs. In *Molecular Replacement*, *Proceedings of the CCP4 Study Weekend*. (Dodson, E.J., Glover, S. & Wolf, W., eds), pp. 92–105, SERC, Daresbury Laboratory, Warrington, UK.
65. Kleywegt, G.J. & Jones, T.A. (1994). Halloween ... Masks and Bones. In *From First Map to Final Model*, *Proceedings of the CCP4 Study Weekend*. (Bailey, S., Hubbard, R. & Waller, D., eds), pp. 59–66, Daresbury Laboratory, Warrington, UK.
66. Jones, T.A., Zou, J.-Y., Cowan, S.W. & Kjelgaard, M. (1991). Improved methods for building protein models in electron density maps and the location of errors in these models. *Acta Cryst.* A **47**, 110–119.
67. Brünger, A.T. (1992). X-PLOR Version 3.1: A system for X-ray crystallography and NMR. Yale University Press, New Haven, CT.
68. Brünger, A.T. (1992). Free R value: a novel statistical quantity for assessing the accuracy of crystal structures. *Nature* **355**, 472–475.
69. Kraulis, P.J. (1991). MOLSCRIPT: a program to produce both a detailed and schematic plots of protein structures. *J. Appl. Cryst.* **24**, 946–950.
70. Bacon, D.J. & Anderson, W.F. (1988). A fast algorithm for rendering space-filling molecule pictures. *J. Mol. Graph.* **6**, 219–220.
71. Merritt, E.A. & Murphy, M.E.P. (1994). Raster3D version 2.0. A program for photorealistic molecular graphics. *Acta Cryst.* D **50**, 869–873.
72. Nicholls, A., Sharp, K.A. & Honig, B. (1991). Protein folding and association: insights from the interfacial and thermodynamic properties of hydrocarbons. *Proteins* **11**, 281–296.
73. Barton, G.J. (1990). Protein multiple sequence alignment and flexible pattern matching. *Methods Enzymol.* **183**, 403–428.
74. Barton, G.J. (1993). ALSCRIPT: a tool to format multiple sequence alignments. *Protein Eng.* **6**, 37–40.
75. Kabsch, W. & Sander, C. (1983). Dictionary of protein secondary structure: pattern recognition of hydrogen-bonded and geometrical features. *Biopolymers* **22**, 2577–2637.